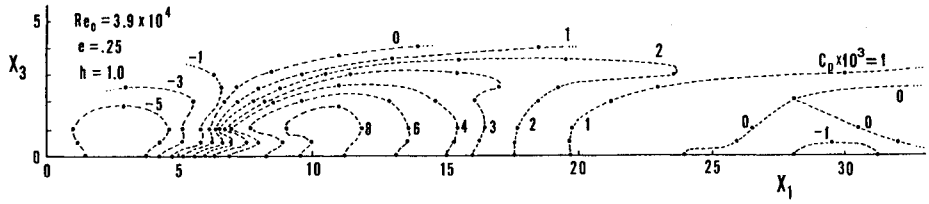


**Fig. 2 Dimensionless surface isopressure map.**

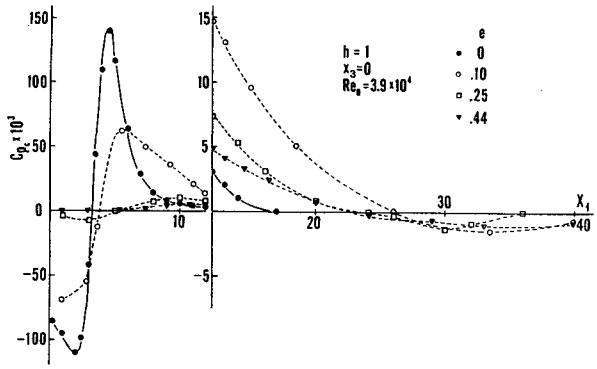


**Fig. 3 Effect of discharge aspect ratio on centerline axial pressure distribution.**

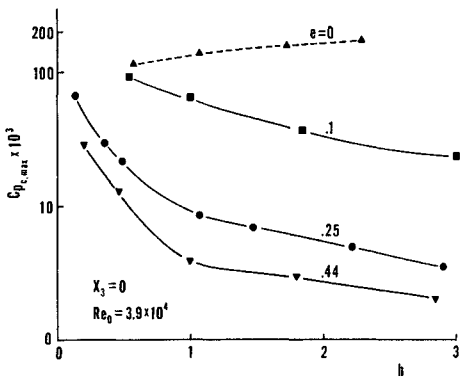


**Fig. 4 Effect of offset distance on the maximum centerline pressure coefficient for two- and three-dimensional jets.**

lower. Furthermore, a decrease in $h$ brings about a decrease in $C_{p,\max}$ for two-dimensional jets, while it causes an increase in $C_{p,\max}$ for three-dimensional jets.

The behavior of surface pressure for small values of $h$ requires careful consideration. For small values of the dimensional offset distance $h^*$ compared to the discharge width $\ell^*$, centerline surface pressure in the vicinity of the discharge should approach that of two-dimensional slot jets. Expressing this ratio in dimensionless form gives $h^*/\ell^* = eh$. Thus, two-dimensional behavior should be approached for $h \ll 1/e$. From this, it follows that the larger the aspect ratio, the smaller $h$ must be to obtain pressure values of two-dimensional jets. This is clear in Fig. 4, which shows that $C_{p,\max}$ occurs in the vicinity of the discharge. For $e = 0.1$, $C_{p,\max}$ approaches its two-dimensional value at $h \simeq 0.5$. At this offset distance, $C_{p,\max}$ for $e = 0.44$ is still an order of magnitude lower than the value corresponding to two-dimensional jets. However, decreasing $h$ further brings the value of $C_{p,\max}$ asymptotically closer to the jets two-dimensional level. In the limiting case of a wall jet ($h = 0$), the pressure throughout the jet is essentially equal to ambient value and, therefore, $C_p = C_{p,\max} \simeq 0$. Thus, at very small values of $h$ (i.e., $h < 0.15$), the $C_{p,\max}$ curves for all aspect ratios should coalesce into as single curve along which $C_{p,\max}$ decreases as $h$ is decreased (two-dimensional behavior) and vanishes at $h = 0$. It was not possible to verify this asymptotic behavior with the present experimental apparatus.

## Conclusions

In general, surface pressure distribution for three-dimensional jets can differ signficantly from two-dimensional jets. However, the centerline surface pressure distribution for three-dimensional jets approaches that of two-dimensional jets at $h \ll 1/e$.

The negative/positive/negative feature of surface pressure coefficient was found to characterize three-dimensional offset jets. The negative surface pressure following reattachment is confined to lateral distances within the channel half-width, i.e., $x < 1/2e$. The negative pressure peaks just downstream of the discharge and the positive peaks after the reattachment points are enhanced as the aspect ratio and/or offset distance are decreased.

## References

[1]Sacks, S., John, J. E. A., and Marks, C. H., "Interaction of a Three-Dimensional Fluid Jet with a Nearby Wall Boundary," *Proceedings of Thermal Pollution Analysis Conference*, Virginia Polytechnic Institute and State University, Blacksburg, 1974, pp. 96-117.

[2]Hoch, J. and Jiji, L. M., "Two-Dimensional Turbulent Offset Jet-Boundary Interaction," *Journal of Fluids Engineering*, Vol. 103, 1981, pp. 154-161.

[3]Bourque, C. and Newman, B. G., "Re-attachment of a Two-Dimensional Incompressible Jet to an Adjacent Flat Plate," *Aeronautical Quarterly*, Vol. 11, Aug. 1960, pp. 201-232.

[4]Newman, B. G., "The Deflection of Plane Jets by Adjacent Boundaries-Coanda Effect," *Boundary Layer and Flow Control*, Pergamon Press, London, 1961, p. 232.

[5]Parameswaran, V. and Alpay, S. A., "Studies on Reattaching Wall Jets," *Transactions of the CSME*, Vol. 3, No. 2, 1975, pp. 83-94.

[6]Rajaratnam, N. and Subramanya, K., "Plane Turbulent Reattached Wall Jets," *ASCE Journal of Hydraulics Division*, Vol. 94, 1968, pp. 95-112.

[7]Kumada, M., Mabuchi, I. and Oyakawa, K., "Studies in Heat Transfer to Turbulent Jets with Adjacent Boundaries, Third Report," *Bulletin of the JSME*, Vol. 16, Nov. 1973, pp. 1712-1722.

# Transient Induced Drag

D. Weihs* and J. Katz†
*NASA Ames Research Center, Moffet Field, California*

## Introduction

A FUNDAMENTAL problem of unsteady aerodynamics is the calculation of forces on a wing that is suddenly brought into motion at a constant speed. The simplest case (a two-dimensional, thin airfoil in an incompressible fluid) was

Received June 20, 1985; revision received Sept. 28, 1985. This paper is declared a work of the U.S. Government and is not subject to copyright protection in the United States.

*NRC Senior Research Associate; also Professor, Department of Aeronautical Engineering, Technion-Israel Institute of Technology, Haifa, Israel. Member AIAA.

†NRC Senior Research Associate. Member AIAA.

first studied by Wagner[1] in 1925. The Wagner solution was generalized to include gust entry, compressible flow, finite wing span, and flexibility.[2-4] These results can be used to calculate the forces experienced by a lifting surface performing more complicated motions by the superposition of the indicial responses.[5]

References 1-5 do not examine the unsteady potential (induced) drag. A calculation of this contribution to the force balance is presented in this Note.

## Analysis

The "inviscid" drag on lifting surfaces is a result of streamwise vorticity shed into the wake, inducing additional velocity components on the surface. Thus, no induced drag is obtained in steady flow over a two-dimensional airfoil. However, the situation is different in transient motion. Here, two separate contributions to induced velocity can be identified: 1) the starting vortex which has a rapidly decaying influence and 2) the vorticity shed because of spanwise nonuniformity (finite span effects) that grows with elapsed time. The first contribution, which we call starting drag, is independent of the aspect ratio and can be understood by using the following model.

Take a flat plate of chord $c$, at an angle of attack $\alpha_g$ (Fig. 1). At time $t=0$, the plate starts moving at speed $U$. At the instant of starting, the plate has already been accelerated to speed $U$, but no motion has occurred. The only points where vorticity can appear at this time are singular points, such as the sharp leading and trailing edges. In order to find the strength of these "indicial" vortices, we recall Wagner's result for the two-dimensional case: that the lift at time $t=0$ (following the initial "added mass" pulse) is one-half the steady lift. For the flat plate, we assume the lift coefficient dependence on the angle of attack is linear, as in the steady state so that the effective aerodynamic angle of attack $\alpha_a$ at $t=0$ is $\alpha_g/2$, deduced from Wagner's result. But $\alpha_a=\alpha_g-\alpha_i$, where $\alpha_i$ is the induced angle of attack, written as

$$\alpha_i = W_0/U \tag{1}$$

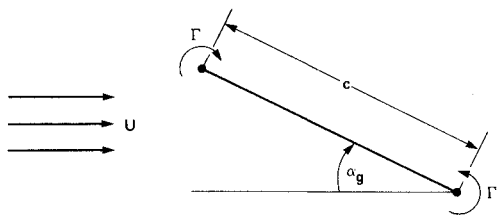


**Fig. 1 Schematic description of flowfield and geometry of the airfoil.**

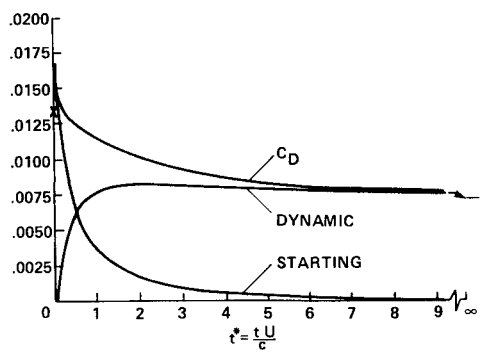


**Fig. 2 Inviscid drag coefficient of a rectangular plate of $\mathcal{R}=8$ at 5 deg angle of attack as a function of nondimensional time. The two effects, impulsive and dynamic, are shown separately. The curves tend to the steady values on the right edge of the figure. X marks the initial value of $C_D$ predicted by Eq. (6).**

where $W$ represents the downwash velocity at each edge of the foil induced by the opposite vortex and the subscript 0 the conditions at time = 0. The induced velocity $W_0$ (on both the leading and trailing edges) can be computed by using the expression for the normal velocity (Ref. 6, Chap. 1) induced by a two-dimensional vortex line $\Gamma$ at a distance $c$, as shown in Fig. 1,

$$W_0 = \Gamma_0/2\pi c \tag{2}$$

As stated previously,

$$\alpha_i = \frac{\alpha_g}{2} = \frac{C_{\ell\infty}}{4\pi} = \frac{1}{4\pi}\,\frac{\rho U\Gamma_\infty}{(\tfrac{1}{2})\rho U^2 c} = \frac{\Gamma_\infty}{2\pi c U} \tag{3}$$

where $C_{\ell\infty}$ is the section steady lift coefficient at time $\to\infty$, so that, combining Eqs. (1-3),

$$\Gamma_0 = \Gamma_\infty \tag{4}$$

Thus, in this model, the total bound vorticity is produced at the initial impulse. This approach, when generalized to finite times, can be used as an alternative to the indicial approach for unsteady aerodynamics and will be reported in detail in the future. For our present purpose, it is sufficient to note that (Ref. 6, Chap. 3)

$$D = \rho W\Gamma \tag{5}$$

where $D$ is the induced drag per unit span. If we rewrite this equation in terms of coefficients and substitute Eqs. (3) and (4), we obtain, for the induced drag at the inception of motion,

$$C_{D_0} = \frac{\rho U\Gamma_\infty}{(\tfrac{1}{2})\rho U^2 c}\,\frac{W_0}{U} = C_{\ell\infty}\,\frac{C_{\ell\infty}}{4\pi} = \frac{C_{\ell\infty}^2}{4\pi} \tag{6}$$

This result, as mentioned previously, is independent of the wing aspect ratio. As time increases, this effect on the drag force becomes smaller as the vortex emanating from the trailing edge is left behind, becoming vanishingly small for large times. The second contributor to induced drag is the spanwise vorticity shedding that results from the spanwise load distribution of three-dimensional wings. This contribution grows with time as the length of the wake grows.

Detailed computations of the variation of the induced drag, with elapsed time from the impulsive start, have been performed using an unsteady lifting surface code.[7] In this program, the forces are obtained by integration of the pressure field over the wing surface, the pressure field being obtained from the unsteady Bernoulli's equation. For incompressible flows, the pressure integral includes only the dynamic $[(\rho/2)U^2]$ and the impulsive $(\partial\phi/\partial t)$ terms.[6] These two contributions are shown in Fig. 2 for a rectangular flat plate of $\mathcal{R}=8$ at angle of attack $\alpha_g=5$ deg.

Figure 3 shows the effect of the aspect ratio on the variation of $C_D$ vs the elapsed time from the impulsive start. The unsteady starting component of the drag (two-dimensional) is almost equal to the steady, induced drag of an elliptical wing of $\mathcal{R}=4$. Thus, as observed, the rectangular wing of $\mathcal{R}=4$ in Fig. 2 would exhibit an almost constant drag coefficient. The initial induced drag, as obtained by Eq. (6), is shown by the X mark in Fig. 2. The difference between this simple model and the more detailed computation of Ref. 7 is caused both by the approximate nature of the model of Eqs. (1-4) and the fact that the induced drag of the rectangular wing is higher than that of an elliptical wing of equal aspect ratio assumed in this model. Also, the numerical technique used is less accurate at times too close to the impulsive start, $t^*=\mathcal{O}(10^{-1})$, where $t^*=tU/c$.

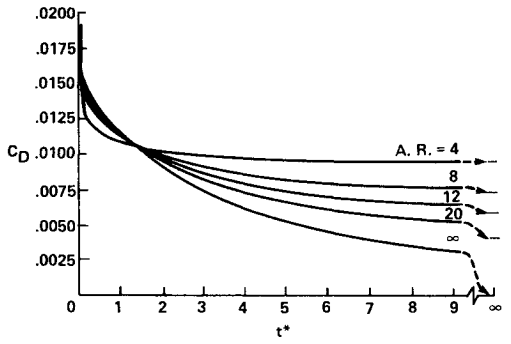


**Fig. 3 Inviscid drag coefficient of rectangular plates of varying aspect ratio as a function of nondimensional time.**

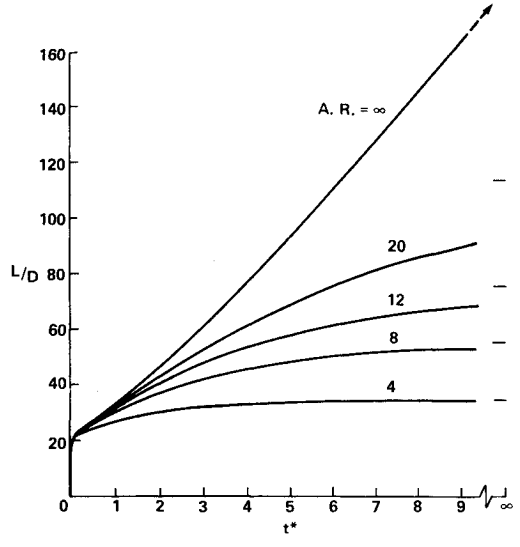


**Fig. 4 Lift-to-inviscid-drag ratio for the planforms of Fig. 3. The curve for the two-dimensional airfoil ($AR=\infty$) tends to infinity as $C_{Di}=0$ for the steady case.**

Another result of the starting drag component is that the induced drag grows faster than the lift. This is shown in Fig. 4, where the inviscid lift-to-drag ($L/D$) ratios for the wings are shown. All of the curves exhibit monotonic growth as a function of time. Had the lift been the faster-growing function, $L/D$ would have had a decreasing dependence on the elapsed time.

## References

[1]Wagner, H., "Uber die Entstehung des Dynamischen Auftriebes von Tragflugeln," *Zeitschrift fuer Angewandte Mathematik und Mechanik*, Vol. 5, No. 1, Feb. 1925, pp. 17-35.

[2]Von Karman, T. and Sears, W. R., "Airfoil Theory for Non-Uniform Motion," *Journal of the Aeronautical Sciences*, Vol. 5, No. 10, Aug. 1938, pp. 370-390.

[3]Lomax, H., Heaslet, M. A., Fuller, F. B., and Sluder, L., "Two and Three Dimensional Problems in High Speed Flight," NACA Rept. 1077, 1953.

[4]Katz, J. and Weihs, D., "The Effect of Chordwise Flexibility on the Lift of a Rapidly Accelerated Airfoil," *Aeronautical Quarterly*, Vol. 30, Feb. 1979, pp. 360-369.

[5]Tobak, M., "On the Use of the Indicial Function Concept in the Analysis of Unsteady Motions of Wings and Wing-Tail Combinations," NACA Rept. 1188, 1954.

[6]Robinson, A. and Laurmann, J. A., *Wing Theory*, Cambridge University Press, London, 1956.

[7]Katz, J., "Large-Scale Vortex-Lattice Model for the Locally Separated Flow over Wings," *AIAA Journal*, Vol. 20, Dec. 1982, pp. 1640-1646.

# Unified Supersonic/Hypersonic Similitude for Oscillating Wedges and Plane Ogives

Kunal Ghosh*
*Indian Institute of Technology, Kanpur, India*

## Introduction

THE large deflection hypersonic similitude of Ghosh[1] was applied by Ghosh and Mistry[2] to the case of an oscillating wedge and plane ogive (nonplanar wedge) to obtain a closed-form expression for the pitching moment derivative due to the rate of pitch $Cm_q$. This derivative had been denoted $Cm_{\dot{\alpha}}$ in Ref. 2 due to a later discovered error in the nomenclature and the similitude extended to oscillating delta wings in Ref. 3. In Ref. 4, a similitude for nonslender cones and quasicones has been outlined and the cylindrically symmetric piston motion of Sedov[5] extended. Hui[6] developed a small-perturbation approach to treat oscillating wedges with attached shocks in supersonic/hypersonic flow. In this Note, a unified supersonic/hypersonic similitude for a wedge and quasiwedge is given. This approach was first reported in abstract form in Ref. 7.

## Steady Wedge

Figure 1 shows the upper half of a wedge at constant-zero incidence with an attached bow shock in rectilinear flight (at time $t$) in stationary inviscid air. The wedge starts its motion at time $t=0$ from point 0. Dimensional analysis indicates that the flow is conical in nature, i.e., at a given instant $\partial/\partial r=0$, where $r$ is the distance along a ray from the apex. Therefore, the bow shock must coincide with a ray. The space-fixed coordinate system $(x,y)$ is so chosen that the $x$ axis coincides with the bow shock at time $t=0$. The conicality of the flow implies that the streamlines at an instant $t$ have the same slope where they intersect a particular ray from the apex. Since the shock sets the fluid particles in a motion normal to itself, the instantaneous streamlines must intersect the shock at right angles. The dashed lines in Fig. 1 are the probable streamline shapes. We tentatively assume that the streamlines are straight as shown by the solid lines in Fig. 1; if this leads to $\partial/\partial r=0$, then it is a solution. Consider the plane flow on a stream surface $x=0$. At time $t$, the shock location on $x=0$ is

$$y_s = U_\infty t\sin\beta \tag{1a}$$

and it can be shown from geometry that the body location is

$$y_b = OB = U_\infty t\sin\delta/\cos\varphi \tag{1b}$$

Since the inviscid flow in plane $x=0$ is independent of the flow in a neighboring parallel plane, it can be taken as a piston-driven fluid motion where the piston velocity is $dy_b/dt$ and hence the piston Mach number is

$$M_p = M_\infty\sin\delta/\cos(\beta-\delta) \tag{1c}$$

The shock Mach number in this plane of motion is $M_s=M_\infty\sin\beta$. Since the piston velocity is independent of time, $\partial p/\partial y=0$. Since the streamlines are straight, there is no centrifugal force on the fluid particles. Hence, $\partial p/\partial x=0$ and $\partial p/\partial r=0$. Thus, the wedge flow is exactly equivalent to one-

Received June 27, 1985; revision received Sept. 16, 1985. 

*Assistant Professor, Department of Aeronautical Engineering.